UNIVERSITY OF BIRMINGHAM

Research at Birmingham

Pd nanoparticle-decorated Bi4O5Br2 nanosheets with enhanced visible-light photocatalytic activity for degradation of bisphenol A

Li, Ning; Zhu, Gangqiang; Hojamberdiev, Mirabbos; Guo, Quanmin

DOI:
10.1016/j.jphotochem.2018.01.029

License:
Creative Commons: Attribution-NonCommercial-NoDerivs (CC BY-NC-ND)

Document Version
Peer reviewed version

Citation for published version (Harvard):
Li, N, Zhu, G, Hojamberdiev, M & Guo, Q 2018, 'Pd nanoparticle-decorated Bi4O5Br2 nanosheets with enhanced visible-light photocatalytic activity for degradation of bisphenol A', Journal of Photochemistry and Photobiology, A: Chemistry, vol. 356, pp. 440-450. https://doi.org/10.1016/j.jphotochem.2018.01.029

Link to publication on Research at Birmingham portal

Publisher Rights Statement:
Checked for eligibility: 27/03/2018
https://doi.org/10.1016/j.jphotochem.2018.01.029

General rights
Unless a licence is specified above, all rights (including copyright and moral rights) in this document are retained by the authors and/or the copyright holders. The express permission of the copyright holder must be obtained for any use of this material other than for purposes permitted by law.

• Users may freely distribute the URL that is used to identify this publication.
• Users may download and/or print one copy of the publication from the University of Birmingham research portal for the purpose of private study or non-commercial research.
• User may use extracts from the document in line with the concept of 'fair dealing' under the Copyright, Designs and Patents Act 1988 (?)
• Users may not further distribute the material nor use it for the purposes of commercial gain.

Where a licence is displayed above, please note the terms and conditions of the licence govern your use of this document.

When citing, please reference the published version.

Take down policy
While the University of Birmingham exercises care and attention in making items available there are rare occasions when an item has been uploaded in error or has been deemed to be commercially or otherwise sensitive.

If you believe that this is the case for this document, please contact UBIRA@lists.bham.ac.uk providing details and we will remove access to the work immediately and investigate.

Download date: 01. Feb. 2019

Accepted Manuscript

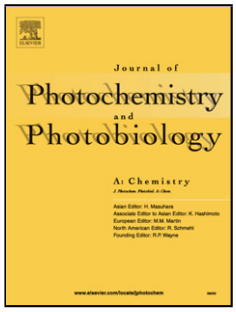

Title: Pd nanoparticle-decorated $Bi_4O_5Br_2$ nanosheets with enhanced visible-light photocatalytic activity for degradation of Bisphenol A

Authors: Ning Li, Gangqiang Zhu, Mirabbos Hojamberdiev, Runliang Zhu, Jun Chang, Jianzhi Gao, Quanmin Guo, Peng Liu

PII: S1010-6030(17)31508-3
DOI: https://doi.org/10.1016/j.jphotochem.2018.01.029
Reference: JPC 11117

To appear in: *Journal of Photochemistry and Photobiology A: Chemistry*

Received date: 13-10-2017
Revised date: 1-1-2018
Accepted date: 18-1-2018

Please cite this article as: Ning Li, Gangqiang Zhu, Mirabbos Hojamberdiev, Runliang Zhu, Jun Chang, Jianzhi Gao, Quanmin Guo, Peng Liu, Pd nanoparticle-decorated Bi4O5Br2 nanosheets with enhanced visible-light photocatalytic activity for degradation of Bisphenol A, Journal of Photochemistry and Photobiology A: Chemistry https://doi.org/10.1016/j.jphotochem.2018.01.029

This is a PDF file of an unedited manuscript that has been accepted for publication. As a service to our customers we are providing this early version of the manuscript. The manuscript will undergo copyediting, typesetting, and review of the resulting proof before it is published in its final form. Please note that during the production process errors may be discovered which could affect the content, and all legal disclaimers that apply to the journal pertain.

ACCEPTED MANUSCRIPT

Pd nanoparticle-decorated $Bi_4O_5Br_2$ nanosheets with enhanced visible-light photocatalytic activity for degradation of Bisphenol A

Ning Li[a], Gangqiang Zhu[a,*], Mirabbos Hojamberdiev[a,c], Runliang Zhu[b], Jun Chang[a], Jianzhi Gao[a], Quanmin Guo[a] and Peng Liu[a]

[a]*School of Physics and Information Technology, Shaanxi Normal University, Xi'an 710062, PR China*

[b]*Guangdong Provincial Key Laboratory of Mineral Physics and Material Research & Development, Guangzhou Institute of Geochemistry, Chinese Academy of Sciences, Guangzhou 510640, China*

[c]*Department of Natural and Mathematic Sciences, Turin Polytechnic University in Tashkent, Kichik Halqa Yo'li 17, Tashkent 100095, Uzbekistan*

*Corresponding author:

Tel/Fax: +86-29-81530750; Email address: zgq2006@snnu.edu.cn (G. Zhu)

ACCEPTED MANUSCRIPT

Graphical abstract

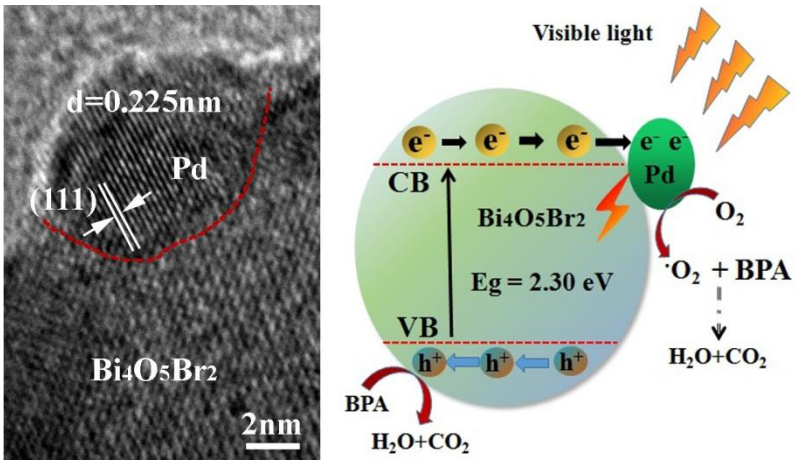

Synopsis: Pd nanoparticles with the size of about 3–6 nm were loaded on the $Bi_4O_5Br_2$ nanosheets with excellent visible-light photocatalytic activity for degradation of Bisphenol A

Highlights

- Pd nanoparticles-loaded ultra-thin $Bi_4O_5Br_2$ nanosheet is reported.
- Pd/$Bi_4O_5Br_2$ showed high photocatalytic activity for Bisphenol A under visible light irradiation.
- Pd/$Bi_4O_5Br_2$ effectively promote the migration of photogenerated charge carriers.

ABSTRACT:

Bismuth oxyhalides are important visible-light-responsive photocatalysts due to their unique

ACCEPTED MANUSCRIPT

electronic and layered crystal structure. In this study, Pd nanoparticles with the size of about 3–6 nm were loaded on the $Bi_4O_5Br_2$ nanosheets by applying solvothermal-reduction method. The photoelectrochemical performance and photocatalytic activity for the degradation of Bisphenol A in aqueous solution of $Bi_4O_5Br_2$ and $Pd/Bi_4O_5Br_2$ were evaluated. Compared with pure $Bi_4O_5Br_2$, $Pd/Bi_4O_5Br_2$ exhibited an excellent photocatalytic activity for the degradation of Bisphenol A in aqueous solution under LED visible light irradiation. 1.0 wt% loading of Pd was found to be most effective for improving the photocatalytic activity of $Bi_4O_5Br_2$ for the degradation of Bisphenol A and near to 95.8% of degradation was achieved after 70 min LED visible light irradiation. Under 535 and 630 nm monochromatic LED visible light irradiation for 70 min, only 7.9% and 4.8% Bisphenol A were degraded over 1.0% $Pd/Bi_4O_5Br_2$ photocatalysts, respectively. Therefore, the improved photocatalytic activity of $Pd/Bi_4O_5Br_2$ is mainly attributed to the formation of a Schottky barrier between the Pd nanoparticles and the $Bi_4O_5Br_2$ nanosheet, promoting efficient separation of photogenerated electrons and holes.

KEYWORDS:

Bismuth oxyhalides; Layered structure; Visible light; Photocatalytic activity; Organic pollutant

1. INTRODUCTION

Bisphenol A (BPA) is an important chemical raw material and widely used as monomer for the

ACCEPTED MANUSCRIPT

production of polycarbonate plastics and epoxy resins [1–3].A large amount of BPA is released into the aquatic environment during its production, causing various diseases such as cancer [4], ovarian disease in women [5], thyroid hormone disruption [6], endocrine disorders, and obesity. In recent years, a number of chemical or physical technologies, including biological degradation [7], thermal decomposition, adsorption [8], ultra-filtration [9], chemical oxidation [10], have been developed for the removal of toxic organic compounds from industrial wastewaters. Among them, photocatalysis is one of the green technologies that utilizes solar light for the complete degradation of organic pollutants and has the potential for environment remediation applications [10-12]. Thus, the development of new, highly efficient photocatalysts is highly desirable from the viewpoint of using solar energy to solve environmental pollution.

Bismuth oxyhalides $Bi_xO_yX_z$ (X = Cl, Br, I) have been intensively studied due to their excellent electrical, optical, and photoluminescence properties [13-16]. Recently, these bismuth oxyhalides have received much attention for their photocatalytic ability in degrading organic pollutants under visible light irradiation because of their unique layered structures with an internal static electric field perpendicular to each layer, which can promote the effective separation of photogenerated electron–hole pairs [13,14,17,18]. Moreover, the variation in the x:y:z values of these compounds can result in significantly different photocatalytic activities [19-21]. As a member of the bismuth-rich bismuth oxyhalides, $Bi_4O_5Br_2$ is of growing interest owing to its narrow band-gap and stable chemical energy and exhibits excellent photocatalytic activity for the degradation of organic pollutants [22-25], H_2 evolution [26], and CO_2 photoreduction [27]. Density functional theory (DFT) calculations showed that the conduction band minimum of $Bi_4O_5Br_2$ primarily consists of the Bi 6p orbital, whereas the valence band maximum is mainly composed of the hybrid orbital of O 2p, and Br 4p [25]. In addition, theoretical and experimental studies demonstrated that the bismuth-rich

ACCEPTED MANUSCRIPT

strategy can increase the conduction band minimum potential of bismuth-rich $Bi_xO_yX_z$ [28]. Therefore, $Bi_4O_5Br_2$ is expected to display higher photocatalytic activity than BiOBr.

In order to further improve the visible-light-induced photocatalytic activity of the $Bi_4O_5Br_2$ nanostructures, several works have been done by coupling with other semiconductors to form heterojunctions such as $C_3N_4/Bi_4O_5Br_2$ [29], $Bi_4O_5Br_2/Bi_{24}O_{31}Br_{10}/Bi_2SiO_5$ [30], and $BN/Bi_4O_5Br_2$ [31]. The heterojunction can significantly reduce the recombination rate and increase the separation rate of photogenerated charge carriers, and the composite photocatalysts become photocatalytically more active than the individual counterparts. In previous reports, highly dispersed novel metal nanoparticles (e.g., Au, Ag, Pd, etc.) loaded on the surfaces of semiconducting materials exhibited extraordinarily high photocatalytic activity for the degradation of organic contaminants [32-34]. The incorporation of noble metal nanoparticles into semiconducting materials can effectively improve photocatalytic performance due to the formation of a Schottky barrier at the interface, which serves as an electron trap. Therefore, it can greatly promote the separation efficiency of photogenerated electrons and holes and increase the photocatalytic activity. Moreover, the noble metal nanoparticles have a wide range of absorption spectrum in the visible light region because of the surface plasmon resonance (SPR), which is defined as the collective oscillation of the conduction electrons [35,36]. Thus, the noble metal nanoparticles/semiconductor composite should have higher photocatalytic activity than the individual semiconductors.

Herein, Pd nanoparticles with the size of about 3–6 nm were loaded on the $Bi_4O_5Br_2$ nanosheets by solvothermal-reduction method to improve the photocatalytic activity of $Bi_4O_5Br_2$. The photoelectrochemical performance and photocatalytic activity for the degradation of Bisphenol A in aqueous solution of $Pd/Bi_4O_5Br_2$ were investigated in comparison to $Bi_4O_5Br_2$. Possible mechanisms for the improved photocatalytic activity for the degradation of Bisphenol A of

ACCEPTED MANUSCRIPT

$Pd/Bi_4O_5Br_2$ are discussed in detail on the basis of the obtained experimental data.

2. EXPERIMENTAL

2.1. Synthesis

2.1.1. Synthesis of $Bi_4O_5Br_2$ nanosheets

$Bi_4O_5Br_2$ nanosheets were synthesized by a hydrothermal method. Typically, 7 mmol of $Bi(NO_3)_3{\cdot}5H_2O$ (>99%, Sinopharm Chemical Reagent Co., Ltd.) and 3.5 mmol of cetyltrimethyl ammonium bromide (CTAB) (>99%, Sinopharm Chemical Reagent Co., Ltd.) were dissolved in 50 mL of deionized water under magnetic stirring at room temperature. 4 mL of NaOH aqueous solution (Sinopharm Chemical Reagent Co., Ltd.) was added dropwise under vigorous stirring, and the precipitates were formed. The suspension was then transferred into an 80 mL Teflon-lined stainless steel autoclave and maintained at 160°C for 12 h. After cooling the autoclave gradually, the resulting precipitates were collected by filtration, washed several times with deionized water, and dried at 60°C for 12 h.

2.1.2. Synthesis of the $Pd/Bi_4O_5Br_2$ composite

$Pd/Bi_4O_5Br_2$ composite was prepared by a reduction method with different loading of Pd nanoparticles (0.5, 1.0, 2.0, and 3.0 wt%). In a typical synthesis process, a certain amount of $Bi_4O_5Br_2$ powder was dispersed in 30 mL of deionized water by ultrasonication and magnetic stirring. Then, K_2PdCl_2 (99.99%, Sigma-Aldrich) aqueous solution (0.06 M) was introduced into the $Bi_4O_5Br_2$–containing suspension, and 30 mL of 1% hydrazine hydrate (Sinopharm Chemical Reagent Co., Ltd.) was subsequently added to the suspension under magnetic stirring for 1 h. The collected powders were washed with deionized water for several times and dried at 60°C for 6 h.

2.2. Characterization

ACCEPTED MANUSCRIPT

The X-ray diffraction (XRD) patterns were recorded on a powder X-ray diffractometer (Bruker D8) with Cu Kα (λ = 1.5406 Å) radiation. The UV–Vis diffuse reflectance spectra (UV–Vis DRS) of the samples were measured by a Cary 5000 UV–VIS–NIR spectrophotometer (Agilent) in the wavelength range of 200–800 nm, and $BaSO_4$ was used as a reference. The transmission electron microscopic (TEM) and high-resolution transmission electron microscopic (HRTEM) images of the samples were taken with a JEM-2100 electron microscope (JEOL) with an acceleration voltage of 200 kV. The chemical states of the elements present in the samples were analyzed by using an Escalab MKII X-ray photoelectron spectrometer (XPS, VG Scienta) with Mg Kα radiation. The morphologies of the samples were observed by field-emission scanning electron microscopy (FE-SEM, Nova NanoSEM 450, FEI) equipped with an energy-dispersive X-ray spectroscopy (EDS) operated at an acceleration voltage of 10 kV. The Brunauer–Emmett–Teller (BET)-specific surface areas of the samples were measured by a N_2 gas adsorption method using an ASAP 2020 instrument (Micromeritics).

2.3. Photocatalytic activity test

The photocatalytic activities of the prepared samples were evaluated toward the photodegradation of Bisphenol A in aqueous solution at ambient temperature. The PCX50A Discover (Perfect Light Co., Ltd.) multi-channel parallel photocatalytic reaction system with a 5 W white LED light (400 nm $\leq \lambda \leq$ 800 nm) was used. In detail, 0.05 g of the prepared sample was dispersed in 50 mL of Bisphenol A aqueous solution (20 mg·L^{-1}) in a glass reactor. Prior to irradiation, the suspension was kept in the dark for 30 min to ensure adsorption-desorption equilibrium. During the photocatalytic reaction, 2 mL of suspension was taken out at certain time intervals for subsequent analysis of the concentration of Bisphenol A in aqueous solution by a U-3010 UV–Vis spectrophotometer (Hitachi).

3. RESULTS AND DISCUSSION

ACCEPTED MANUSCRIPT

3.1. XRD

Fig. 1a shows the XRD patterns of $Bi_4O_5Br_2$ and $Pd/Bi_4O_5Br_2$ samples, indicating strong diffraction peaks at 2θ = 24.29, 29.54, 31.80, 32.86, and 45.49°. These diffraction peaks correspond to the (112), (11-3), (020), (021), and (422) planes of tetragonal $Bi_4O_5Br_2$ with space group of $P_{21}(4)$ (ICDD card no. 37–0699). As can be seen, no diffraction peaks belonging to any impurity phases are detected in the XRD patterns. The diffraction peaks of Pd nanoparticles are also absent in the XRD pattern of $Pd/Bi_4O_5Br_2$ composite possibly due to the low concentration and high dispersion of Pd nanoparticles in the composite. Although the XRD pattern of $Pd/Bi_4O_5Br_2$ composite does not provide enough evidence for the presence of Pd nanoparticles in the composite, the yellow color of the $Bi_4O_5Br_2$ powders apparently turned to gray after loading the Pd nanoparticles, as shown in Fig. 1a. As illustrated in Fig. 1b, the $Bi_4O_5Br_2$ possesses a layered crystal structure with the $[Bi_2O_2]^{2+}$ and Br^- slices stacked together by the non-bonding interaction through the Br atoms along the *c*-axis to form the unique layered structure. This layered structure is indicative of the existence of the self-induced electric field in $Bi_4O_5Br_2$, which promotes effective separation of photogenerated electron-hole pairs [13,14].

3.2. XPS

To investigate the chemical states of the elements, 1.0 wt% $Pd/Bi_4O_5Br_2$ composite was analyzed by X-ray photoelectron spectroscopy (XPS). Fig. 2a shows the XPS survey spectrum of the composite, which consists of Bi, O, Br and Pd. The high-resolution XPS spectra of Bi 4f in Fig. 2b showed that the binding energy of pure $Bi_4O_5Br_2$ and 1.0 wt% $Pd/Bi_4O_5Br_2$ composite were the same. The two symmetric peaks centered at 158.8 and 164.2 eV correspond to the typical binding energies of Bi $4f_{7/2}$ and Bi $4f_{5/2}$ [10], respectively. This revealed that Pd nanoparticles deposition did not affect the valence state of the surface atoms of $Bi_4O_5Br_2$. Fig. 2c shows the asymmetric O 1s

ACCEPTED MANUSCRIPT

XPS spectra that are deconvoluted into two symmetric peaks by using an XPS peak-fitting software. The peak at 529.6 eV is assigned to oxygen in the Bi–O of $Bi_4O_5Br_2$ [10,24], whereas the peak at 531.3 eV is associated with the external –OH group or water molecules adsorbed on the surface of the sample [21,36]. As shown in Fig. 2d, the peaks observed at around 68.4 eV are attributed to the Br 3d doublet. Fig. 2e shows two asymmetric peaks in the range of 333.6–343.8 eV. The main XPS peaks located at 335.3 and 340.6 eV are assigned to Pd $3d_{5/2}$ and Pd $3d_{3/2}$ of metal Pd nanoparticles [37], respectively. In addition, the peaks located at 336.8 and 342.1 eV are related to Pd $3d_{5/2}$ and Pd $3d_{3/2}$ of Pd^{2+} in 1.0 wt% Pd/$Bi_4O_5Br_2$ composite [37], respectively.

3.3. TEM

The morphology and microstructure of the prepared samples were investigated by TEM. The TEM and HRTEM images of the $Bi_4O_5Br_2$ powders are shown in Fig. 3a and 3b, respectively. It is clear from Fig. 3a that the $Bi_4O_5Br_2$ particles are composed of ultra-thin nanosheets with the thickness of about 9 nm. The HRTEM image of an individual nanosheet of the $Bi_4O_5Br_2$ sample is shown in Fig. 3b, confirming its single-crystalline nature. It can be seen that the $Bi_4O_5Br_2$ crystallites have distinct lattice spacings of about 0.276 nm, corresponding to the (120) crystallographic planes. Fig. 3c shows the TEM image of the 1.0 wt% Pd/$Bi_4O_5Br_2$ composite, indicating that many Pd nanoparticles with the size of about 3–6 nm are distributed on the surfaces of the $Bi_4O_5Br_2$ nanosheets. The HRTEM images in Fig. 3e-g indicate that two different lattice fringes of 0.276 and 0.225 nm can be observed, which correspond to the (120) plane of $Bi_4O_5Br_2$ and the (111) plane of Pd, respectively. Integrated with the above-given XPS, TEM, and HRTEM results, it can be deduced that the Pd nanoparticles were successfully deposited on the surfaces of the $Bi_4O_5Br_2$ nanosheets.

3.4. EDS

ACCEPTED MANUSCRIPT

The elemental composition and distribution of 1.0 wt% Pd/$Bi_4O_5Br_2$ composite were analyzed by energy dispersive X-ray spectroscopy (EDS). Fig. 4 shows the SEM image, EDS spectrum, and EDS element mapping images of O, Bi, Br, and Pd of 1.0 wt% Pd/$Bi_4O_5Br_2$. Fig. 4a clearly shows that the $Bi_4O_5Br_2$ particles were assembled by ultra-thin nanosheets, and the EDS spectrum in Fig. 4b confirms the presence of Bi, O, Br, and Pd in the prepared composite. In addition, the EDS element mapping images shown in Fig. 4c-f suggest homogenous distribution of Bi, O, Br, and Pd in the prepared composite.

3.5. UV-Vis DRS

The UV-Vis diffuse reflectance spectra of the prepared samples are shown in Fig. 5a. The $Bi_4O_5Br_2$ shows a light absorption from the UV to visible light region, and the wavelength of the absorption edge is about 488 nm, implying that $Bi_4O_5Br_2$ can be applied in the visible-light-induced photocatalytic reactions. As noticed, the presence of Pd nanoparticles enhanced the absorption ability of the $Bi_4O_5Br_2$ powders in the visible-light region, and the absorption intensity of the prepared composites was increased with increasing Pd loading. The optical band-gap energies of the prepared samples were estimated by using Eq. (1)

$$\alpha h\nu = A\left(h\nu - E_g\right)^{n/2} \quad (1)$$

where α, h, ν and E_g are the absorption coefficient, Planck constant, light frequency, and band gap energy, respectively. A in the equation (1) is just a constant. According to Eq. (1), n is determined from the type of an optical transition of semiconductor (n = 1 for direct transition, and n = 4 for indirect transition). The optical band-gap energy of the $Bi_4O_5Br_2$ powders is estimated to be about 2.30 eV (Fig. 5b).

3.6. Surface area

The surface area of the as-prepared samples was investigated by N_2 adsorption and desorption

ACCEPTED MANUSCRIPT

isotherms. Fig. 6 shows the nitrogen adsorption–desorption isotherms for pure $Bi_4O_5Br_2$, 0.5 wt% $Pd/Bi_4O_5Br_2$, 1.0 wt% $Pd/Bi_4O_5Br_2$, 2.0 wt% $Pd/Bi_4O_5Br_2$ and 3.0 wt% $Pd/Bi_4O_5Br_2$ samples. The isotherms of all the samples can be classified as type IV, possessing a distinct H3-type hysteresis loop. The BET specific surface area (S_{BET}) of the pure $Bi_4O_5Br_2$, 0.5wt% $Pd/Bi_4O_5Br_2$, 1.0wt% $Pd/Bi_4O_5Br_2$, 2.0wt% $Pd/Bi_4O_5Br_2$ and 3.0wt% $Pd/Bi_4O_5Br_2$ are 15.16, 18.45, 20.09, 21.00 and 22.83 m^2/g, respectively. From the above results, it can be seem that the surface area of the samples increased with increasing the amount of Pd phase in the composite.

3.7. Photocatalytic activity

The photocatalytic activities of the $Bi_4O_5Br_2$ and $Pd/Bi_4O_5Br_2$ samples were evaluated by the degradation of Bisphenol A under LED visible light irradiation. The temporal changes of Bisphenol A (BPA) concentration were monitored by examining the variation in the maximum absorption in the UV–Vis spectra of Bisphenol A aqueous solution (20 $mg \cdot L^{-1}$) at 276 nm. Fig. 7a shows the variation of the BPA concentration (C/C_0) against photodegradation time over the prepared samples. An additional experiment was also performed for the direct photolysis of BPA in the absence of photocatalysts, and no obvious change was observed in the BPA concentration within 70 min of LED visible light irradiation. Meanwhile, the photodegradation of BPA over $Bi_4O_5Br_2$ sample was about 53.3% after 70 min of LED visible light irradiation, indicating that the $Bi_4O_5Br_2$ nanosheets can degrade BPA under visible light irradiation. Clearly, the photocatalytic performance of $Bi_4O_5Br_2$ is significantly improved after loading a suitable amount of Pd nanoparticles. Under the identical experimental conditions, the photodegradation of BPA over $Pd/Bi_4O_5Br_2$ composites loaded with 0.5, 1.0, 2.0, and 3.0 wt% Pd nanoparticles is 87.0, 95.8, 67.2, and 51.4%, respectively. In order to quantitatively understand the reaction kinetics of the BPA degradation over the prepared samples, the pseudo-first order was used to fit the experimentally obtained data. The pseudo-first

ACCEPTED MANUSCRIPT

order is expressed as $\ln(C_0/C) = kt$, where C_0 and C are the concentrations of BPA in aqueous solution at time 0 (the time to obtain adsorption–desorption equilibrium) and t, respectively, and k is the pseudo-first order rate constant. The pseudo-first order rate constant (k) for the prepared $Bi_4O_5Br_2$ and Pd/$Bi_4O_5Br_2$ samples were calculated based on the data plotted in Fig. 7b. The calculated pseudo-first order rate constant for the prepared samples can be placed in the following sequence according to the content of Pd nanoparticles: 0.0548 min^{-1} for 1.0 wt% > 0.0266 min^{-1} for 0.5 wt% > 0.0156 min^{-1} for 2.0 wt% > 0.0108 min^{-1} for 0.0 wt% > 0.0101 min^{-1} for 3.0 wt%. It is obvious that the presence of a suitable amount of Pd nanoparticles loaded on $Bi_4O_5Br_2$ nanosheets accelerates the photodegradation reaction of BPA under LED visible light irradiation. The degradation rate constant for BPA of 1.0 wt% Pd/$Bi_4O_5Br_2$ is about 5 times higher than that of pure $Bi_4O_5Br_2$. Fig. 7c and d show the UV–Vis spectra of BPA aqueous solution collected during the photocatalytic reactions with $Bi_4O_5Br_2$ and 1.0 wt% Pd/$Bi_4O_5Br_2$, respectively. As shown, the 1.0 wt% Pd/$Bi_4O_5Br_2$ composite shows higher photocatalytic activity for the degradation of BPA than $Bi_4O_5Br_2$.

In recent years, the composite photocatalysts developed by loading metal nanoparticles (e.g., Bi, Au, Ag and Pd) on semiconductor nanostructures attracted much attention due to their enhanced visible light photocatalytic activity [38-42]. On one hand, the loading of noble metal nanoparticles on semiconductor nanostructures creates a Schottky barrier that acts as an electron trap, improving the quantum efficiency through efficient separation of photogenerated electron-hole pairs and enhancing the photocatalytic activity. On the other hand, the noble metal nanoparticles can induce localized surface plasmon resonance (LSPR), which improves the light absorption of semiconductor throughout the range from visible to near-infrared and transfers the plasmonic energy from the noble metal to the semiconductor. More importantly, the size of the noble metal nanoparticles plays

ACCEPTED MANUSCRIPT

an essential role in determining the photocatalytic efficiency of the developed composite photocatalyst [43,44]. In previous report, larger noble metal nanoparticles (≥ 10 nm) were reported to result in a superior photocatalytic activity under visible light irradiation due to stronger surface plasmonic resonance [45].

In order to investigate the LSPR effect of the Pd nanoparticles with the size of 3–6 nm in the prepared composite, the photocatalytic activities of the $Bi_4O_5Br_2$ and 1.0 wt% Pd/$Bi_4O_5Br_2$ samples for the degradation of BPA under monochromatic 420, 450, 535, and 630 nm LED visible light irradiation were also investigated here, and the results are plotted in Fig. 8. Under 420 and 450 nm monochromatic LED visible light irradiation (Fig. 8a), the $Bi_4O_5Br_2$ sample showed slightly higher photocatalytic activity (74.8%) than under white LED light irradiation (63.7%) for the degradation of BPA within 70 min. Obviously, when the wavelength of the monochromatic LED light exceeds 535 nm, the photodegradation efficiency of BPA over $Bi_4O_5Br_2$ becomes negligible (Fig. 8a). It can be seen from Fig. 8b that the 1.0 wt% Pd/$Bi_4O_5Br_2$ composite exhibited excellent photocatalytic activity for the degradation of BPA under 420 and 450 nm monochromatic LED visible light irradiation. Especially, about 99.9% BPA was degraded under 420 nm monochromatic LED visible light irradiation. Interestingly, increasing the wavelength of the monochromatic light to 535 nm, the photodegradation efficiency of BPA over 1.0 wt% Pd/$Bi_4O_5Br_2$ composite gradually declined within 70 min. Only 7.9% and 4.8% BPA were degraded under 535 and 630 nm monochromatic LED visible light irradiation for 70 min, respectively (Fig. 8c). Fig. 8d shows the pseudo-first order rate constants (k) for the $Bi_4O_5Br_2$ and Pd/$Bi_4O_5Br_2$ samples under monochromatic 420, 450, 535, and 630 nm LED visible light irradiation. From the results shown in Fig. 8, a weak LSPR effect on photocatalytic activity of 1.0 wt% Pd/$Bi_4O_5Br_2$ composite was noticed. Notably, the 1.0 wt% Pd/$Bi_4O_5Br_2$ composite exhibits higher photocatalytic activity than $Bi_4O_5Br_2$ in the visible light

ACCEPTED MANUSCRIPT

region due to the formation of Schottky barrier between the Pd nanoparticles and $Bi_4O_5Br_2$ nanosheets present in the composite.

3.7. Mechanisms

It is well known that the photocatalytic process in the presence of semiconductor involves light photoexcitation, subsequent separation and transfer of photogenerated charge carriers, and final redox reactions between the photogenerated charge carriers and adsorbate on the semiconductor surface. Accordingly, the charge dynamics property plays an important role in determining the photoreactivity of photocatalysts. The separation and transfer of the photogenerated charge carriers in $Bi_4O_5Br_2$ and 1.0 wt% Pd/$Bi_4O_5Br_2$ samples were investigated by photoluminescence spectroscopy (PL) and photoelectrochemical method. The PL spectra of $Bi_4O_5Br_2$ and 1.0 wt% Pd/$Bi_4O_5Br_2$ samples with an excitation wavelength of 325 nm are shown in Fig. 9. As shown in Fig. 9a, the observed peak position and shape of the PL spectrum at around 475 nm are identical for $Bi_4O_5Br_2$ due to the radiative recombination process of e^-/h^+ pairs with emission of photon and self-trapped excitons. However, the same peak in the PL spectrum of 1.0 wt% Pd/$Bi_4O_5Br_2$ sample at around 475 nm nearly disappears. In order to further confirm the separation rate of photo-generated electron-hole pairs, the transient photocurrent responses of both samples were measured under visible light irradiation using a 300 W Xenon lamp with 420 nm cutoff filter through light-on and light-off cycles. In Fig. 9b, the 1.0 wt% Pd/$Bi_4O_5Br_2$ photoelectrode shows a two-fold higher photocurrent density compared with $Bi_4O_5Br_2$ photoelectrode, indicating efficient separation and faster transfer of photo-generated charge carriers.

To further evaluate the role of reactive species, various quenchers have been used to scavenge the relevant reactive species, including hydroxyl radicals (•OH), superoxide anions ($\bullet O_2^-$), hole (h^+), etc. In this work, ammonium oxalate (AO, 1.0 mmol·L^{-1}), isopropanol (IPA, 1.0 mmol·L^{-1}), and

ACCEPTED MANUSCRIPT

ascorbic acid (AA, 1.0 mmol·L^{-1}) were adopted as h^+, •OH, and $•O_2^-$ scavengers during the photodegradation of BPA by 1.0 wt% Pd/$Bi_4O_5Br_2$ under visible light irradiation, respectively, and the corresponding results are shown in Fig. 9c. With the addition of AO, IPA, and AA, about 12.6, 35.8, and 90.7% of BPA were degraded under visible light irradiation. The above results suggested that both h^+ and $•O_2^-$ species, especially the former, play an important role in the photodegradation of BPA over the 1.0 wt% Pd/$Bi_4O_5Br_2$ under visible light irradiation.

As represented in Fig. 9d, possible mechanisms for the photodegradation of BPA over the Pd/$Bi_4O_5Br_2$ can be explained in detail. As for a visible-light-responsive semiconductor, the electrons of the valence band of $Bi_4O_5Br_2$ becomes excited and electron-hole pairs are formed when illuminated by visible light. Once the Pd nanoparticles are deposited on the $Bi_4O_5Br_2$ nanosheets, they act as electron traps to promote the electron-hole separation, and the trapped electrons are subsequently withdrawn by the surface-adsorbed O_2 on the surfaces of the $Bi_4O_5Br_2$ nanosheets to form reactive oxygen species $•O_2^-$. Further, the $•O_2^-$ will oxidize BPA in aqueous solution. Simultaneously, the photo-generated holes in the valence band of $Bi_4O_5Br_2$ will migrate to the surfaces of the photocatalyst and directly oxidize BPA. Hence, the prepared Pd/$Bi_4O_5Br_2$ composite photocatalyst shows improved photocatalytic activity under visible light irradiation compared with $Bi_4O_5Br_2$ and can be applied for the treatment of water contaminated with organic pollutants.

4. CONCLUSIONS

In summary, we have prepared a novel composite photocatalyst by depositing Pd nanoparticles with the size of about 3–6 nm on the $Bi_4O_5Br_2$ nanosheets by applying a solvothermal-reduction method. The photoelectrochemical performance and photocatalytic activity for the degradation of Bisphenol A in aqueous solution of $Bi_4O_5Br_2$ and Pd/$Bi_4O_5Br_2$ with different amounts of Pd nanoparticles were evaluated. Expectedly, the Pd/$Bi_4O_5Br_2$ composite exhibited excellent

ACCEPTED MANUSCRIPT

photocatalytic activity for the degradation of Bisphenol A in aqueous solution under LED visible light irradiation compared with $Bi_4O_5Br_2$. Particularly, 1.0 wt% Pd was found to be efficient for improving the photocatalytic activity of $Bi_4O_5Br_2$. The improved photocatalytic activity of $Pd/Bi_4O_5Br_2$ is attributed to the formation of a Schottky barrier between Pd nanoparticles and $Bi_4O_5Br_2$ nanosheets, promoting an efficient separation of photogenerated electrons and holes. The $Pd/Bi_4O_5Br_2$ composite can be used in water treatment process.

Competing financial interest

The authors declare no competing financial interest.

ACKNOWLEDGMENTS

This work was supported by the National Natural Science Foundation of China (Grant nos. 51772183 and 11474191), the Fundamental Research Funds for the Central Universities (Grant nos. GK201602008 and GK201603013), and the research fund for Guangdong Provincial Key Laboratory of Mineral Physics and Materials (Grant no. GLMPM-017).

ACCEPTED MANUSCRIPT

ACCEPTED MANUSCRIPT

References

[1] J.G. Hengstler, H. Foth, T. Gebel, P.J. Kramer, W. Lilienblum, H. Schweinfurth, W. Volkel, K.M. Wollin, U. Gundert-Remy, Critical evaluation of key evidence on the human health hazards of exposure to bisphenol A, *Crit. Rev. Toxicol*, 2011, 41, 263-291.

[2] H. Melcer, G. Klečka. Treatment of wastewaters containing bisphenol A: State of the science review, *Water. Environ. Res*, 2011, 83, 650-666.

[4] R.A. Keri, S.M. Ho, P.A. Hunt, K.E. Knudsen, A.M. Soto, G.S. Prins, An evaluation of evidence for the carcinogenic activity of bisphenol A, *Reprod. Toxicol*, 2007, 24, 240-252.

[5] T. Takeuchi, O. Tsutsumi, Y. Ikezuki, Y. Takai, Y. Taketani, Positive relationship between androgen and the endocrine disruptor, bisphenol A, in normal women and women with ovarian dysfunction, *Endocr. J*, 2004, 51, 165-169.

[6] R.T. Zoeller, R. Bansal, C. Parris, Bisphenol-A, an environmental contaminant that acts as a thyroid hormone receptor antagonist in vitro, increases serum thyroxine, and alters RC3 /neurogranin expression in the developing rat brain, *Endocrinology*, 2005, 146, 607-612.

[7] M.C. Tomeia, D.M. Angeluccia, V. Stazia, A.J. Daugulis. On the applicability of a hybrid bioreactor operated with polymeric tubing for the biological treatment of saline wastewater, *Sci. Total. Environ*, 2017, 599–600, 1056–1063.

[8] Y. Zhang, G.H. Huang, C.J. An, X.Y. Xin, X. Liu, M. Raman, Y. Yao, W.X. Wang, M. Doble. Transport of anionic azo dyes from aqueous solution to gemini surfactant-modified wheat bran: Synchrotron infrared, molecular interaction and adsorption studies, *Sci. Total. Environ*, 2017, 595, 723–732.

[9] I.M. Atadashi, M.K. Aroua, A.R. AbdulAziz, N.M.N. Sulaiman, Removal of residual palm

ACCEPTED MANUSCRIPT

oil-based biodiesel catalyst using membrane ultra-filtration technique: An optimization study, *Alex. Eng. J*, 2014, 53, 705-715.

[10] Y.B. Liu, G.Q. Zhu, J.Z. Gao, R.L. Zhu, M. Hojamberdiev, C. H. Wang, X.M. Wei, P. Liu. A novel synergy of Er^{3+}/Fe^{3+} co-doped porous Bi_5O_7I microspheres with enhanced photocatalytic activity under visible-light irradiation, *Appl. Catal. B: Environ*, 2017, 205, 421–432.

[11] J. Zita, J. Krysa, A. Mills, Correlation of oxidative and reductive dye bleaching on TiO_2 photocatalyst films, *J. Photochem. Photobiol. A*, 2009, 203, 119–124..

[12] Y.N. Chen, G.Q. Zhu, M. Hojamberdiev, J.Z. Gao, R.L. Zhu, C.H. Wang, X.M. Wei, P. Liu. Three-dimensional Ag_2O/Bi_5O_7I *p–n* heterojunction photocatalyst harnessing UV–Vis–NIR broad spectrum for photodegradation of organic pollutants. *J. Hazard. Mater*, 2018, 344, 42-54..

[13] L.Q. Ye, Y.R. Su, X.L. Jin, H.Q. Xie, C. Zhang. Recent advances in BiOX (X = Cl, Br and I) photocatalysts: synthesis, modification, facet effects and mechanisms, *Environ. Sci.: Nano*, 2014, 1, 90–112.

[14] A. Dash, S. Sarkar, V.N.K.B. Adusumalli, V. Mahalingam. Microwave dynthesis, photoluminescence, and photocatalytic activity of PVA-gunctionalized Eu^{3+}-doped BiOX (X=Cl, Br, I) nanoflakes, *Langmuir*, 2014, 30, 1401-1409.

[15] J. Li, Y. Yu, L.Z. Zhang. Bismuth oxyhalide nanomaterials: layered structures meet photocatalysis, *Nanoscale*, 2014, 6, 8473–8488.

[16] S.M. Sun, W.Z. Wang, L. Zhang, L. Zhou, W.Z. Yin, M. Shang. Visible light-induced efficient contaminant removal by Bi_5O_7I, *Environ. Sci. Technol*, 2009, 43, 2005–2010.

[17] J. Di, J.X. Xia, H.M. Li, S.J. Guo, S. Dai. Bismuth oxyhalide layered materials for energy and environmental applications. *Nano Energy*, 2017, 41, 172-192.

[18] J.X. Xia, J. Di, H.T. Li, H. Xu, H.M. Li, S.J. Guo. Ionic Liquid-Induced Strategy for Carbon

ACCEPTED MANUSCRIPT

Quantum Dots/BiOX (X= Br, Cl) Hybrid Nanosheets with Superior Visible Light-Driven Photocatalysis, *Appl. Catal. B: Environ*, 2016, 181, 260-269.

[19] C.Y. Wang, X. Zhang, H.B. Qiu, W.K. Wang, G.X. Huang, J. Jiang, H.Q. Yu. Photocatalytic degradation of bisphenol A by oxygen-rich and highly visible-light responsive $Bi_{12}O_{17}Cl_2$ nanobelts, *Appl. Catal. B: Environ*, 2017, 200, 659–665.

[20] X. Xiao, C. Liu, R.P. Hu, X.X. Zuo, J.M. Nan, L.S. Li, L.S. Wang. Oxygen-rich bismuth oxyhalides: generalized one-pot synthesis, band structures and visible-light photocatalytic properties, *J. Mater. Chem*, 2012, 22, 22840-22843.

[21] J.L. Han, G.Q. Zhu, M. Hojamberdiev, J.H. Peng, P. Liu. Temperature effect on phase transition and morphological transformation of BiOI microspheres to Bi_5O_7I microstructures, *Mater. Lett*, 2016, 169, 122–125.

[22] M. Li, Y.J. Cui, Y.S. Jin, H. Li, Facile hydrolysis synthesis of $Bi_4O_5Br_2$ photocatalyst with excellent visible light photocatalytic performance for the degradation of resorcinol, *RSC Adv*, 2016, 6, 47545-47551.

[23] J.X. Xia, Y.P. Ge, J. Di, L. Xu, S. Yin, Z.G. Chen, P.J. Liu, H.M. Li. Ionic liquid-assisted strategy for bismuth-rich bismuth oxybromides nanosheets with superior visible light-driven photocatalytic removal of bisphenol-A, *J. Colloid. Interface Sci*, 2016, 473, 112–119.

[24] J. Di, J.X. Xia, M.X. Ji, S. Yin, H.P. Li, H. Xu, Q. Zhang, H.M. Li. Controllable synthesis of $Bi_4O_5Br_2$ ultrathin nanosheets for photocatalytic removal of ciprofloxacin and mechanism insight, *J. Mater. Chem. A*, 2015, 3, 15108–15118.

[25] R. Li, F.X. Xie, J.X. Liu, Y.W. Wang, Y.F. Wang, X.C. Zhang, C.M. Fan. Synthesis of $Bi_4O_5Br_2$ from reorganization of BiOBr and its excellent visible light photocatalytic activity, *Dalton. Trans*, 2016, 45, 9182–9186.

ACCEPTED MANUSCRIPT

[26] Y. Bai, T. Chen, P.Q. Wang, L. Wang, L.Q. Ye. Bismuth-rich $Bi_4O_5X_2$ (X = Br, and I) nanosheets with dominant {101} facets exposure for photocatalytic H_2 evolution, *Chem. Eng. J*, 2016, 304, 454–460.

[27] L.Q. Ye, X.L. Jin, C. Liu, C.H. Ding, H.Q. Xie, K.H. Chu, P.K. Wong. Thickness-ultrathin and bismuth-rich strategies for BiOBr to enhance photoreduction of CO_2 into solar fuels, *Appl. Catal. B: Environ*, 2016, 187, 281–290.

[28] X.L. Jin, L.Q. Ye, H. Wang, Y.R. Su, H.Q. Xie, Z.G. Zhong, H. Zhang. Bismuth-rich strategy induced photocatalytic molecular oxygen activation properties of bismuth oxyhalogen: The case of $Bi_{24}O_{31}Cl_{10}$, *Appl. Catal. B: Environ*, 2015, 165, 668–675.

[29] M.X. Ji, J. Di, Y.P. Ge, J.X. Xia, H.M. Li. 2D-2D stacking of graphene-like g-C_3N_4/Ultrathin $Bi_4O_5X_2$ with matched energy band structure towards antibiotic removal, *Appl. Surf. Sci*, 2017, 413, 372–380.

[30] D. Liu, W.Q. Yao, J. Wang, Y.F. Liu, M. Zhang, Y.F. Zhu. Enhanced visible light photocatalytic performance of a novel heterostructured $Bi_4O_5X_2/Bi_{24}O_{31}Br_{10}/Bi_2SiO_5$ photocatalyst, *Appl. Catal. B: Environ*, 2015, 172–173, 100–107

[31] S.S. Ding, D.J. Mao, S.G. Yang, F. Wang, L.J. Meng, M.S. Han, H. He, C. Sun, B. Xu. Graphene-analogue h-BN coupled Bi-rich $Bi_4O_5X_2$ layered microspheres for enhanced visible-light photocatalytic activity and mechanism insight, *Appl. Catal. B: Environ*, 2017, 210, 386–399.

[32] Y.B. Liu, G.Q. Zhu, J.Z. Gao, M. Hojamberdiev, R.L. Zhu, X.M. Wei, Q.M. Guo, P. Liu. Enhanced photocatalytic activity of $Bi_4Ti_3O_{12}$ nanosheets by Fe^{3+}-doping and the addition of Au nanoparticles: Photodegradation of Phenol and bisphenol A, *Appl. Catal. B: Environ*, 2017, 200, 72–82.

[33] S.H. Nam, H.S. Shim, J.G. Kim, W.B. Kim, Ag or Au Nanoparticle-embedded one-dimensional

ACCEPTED MANUSCRIPT

composite TiO_2 nanofibers prepared via electrospinning for use in lithium-ion batteries, *ACS Appl. Mater. Interfaces*, 2010, 2, 2046-2052.

[34] R.A. Zayadi, F. Abu Bakar. Comparative study on the performance of Au/F-TiO_2 photocatalyst synthesized from Zamzam water and distilled water under blue light irradiation, *J. Photochem. Photobiol. A: Chem*, 2017, 346, 338-350.

[35] Y.C. Pu, G.M. Wang, K.D. Chang, Y.C. Ling, Y.K. Lin, B.C. Fitzmorris, C.M. Liu, X.H. Lu, Y.X. Tong, J.Z. Zhang, Y.J. Hsu, Y. Li, Au nanostructure-decorated TiO_2 nanowires exhibiting photoactivity across entire UV-visible region for photoelectrochemical water splitting, *Nano Lett*, 2013, 13, 3817-3823.

[36] L. Jin, G.Q. Zhu, M. Hojamberdiev, X.C. Luo, J.H. Peng, P. Liu, A plasmonic Ag-AgBr/$Bi_2O_2CO_3$ composite photocatalyst with enhanced visible-light photocatalytic activity, *Ind. Eng. Chem. Res*, 2014, 53, 13718-13727.

[37] X.C. Meng, Z.S. Zhang. Pd-doped Bi_2MoO_6 plasmonic photocatalysts with enhanced visible light photocatalytic performance, *Appl. Surf. Sci*, 2017, 392, 169–180.

[38] Z.Y. Wang, S. Yan, Y.J. Sun, T. Xiong, F. Dong, W. Zhang. Bi metal sphere/graphene oxide nanohybrids with enhanced direct plasmonic photocatalysis, *Appl. Catal. B: Environ*, 2017, 214, 148-157.

[39] Q.Z. Wang, J.J. He, Y.B. Shi, S.L. Zhang, T.J. Niu, H.D. She, Y.P. Bi. Designing of non-noblemiconductor Bi/$BiVO_4$ photoelectrode for enhanced photoelectrochemical performance. *Chem. Eng. J*, 2017, 326, 411-418.

[40] J.Y. Qin, H.P. Zeng. Photocatalysts fabricated by depositing plasmonic Ag nanoparticleson carbon quantum dots/graphitic carbon nitride for broad spectrumphotocatalytic hydrogen generation, *Appl. Catal. B: Environ*, 2017, 209, 161–173

ACCEPTED MANUSCRIPT

[41] J.J. Xue, S.S. Ma, Y.M. Zhou, Z.W. Zhang, M. He. Facile Photochemical Synthesis of Au/Pt/g-C_3N_4 with Plasmon-Enhanced Photocatalytic Activity for Antibiotic Degradation, *ACS Appl. Mater. Interfaces*, 2015, 7, 9630−9637.

[42] Y. Tian, W. Li, C.H. Zhao, Y.F. Wang, B.L. Zhang, Q.Y. Zhang. Fabrication of hollow mesoporous SiO_2-BiOCl@PANI@Pd photocatalysts to improve the photocatalytic performance under visible light, *Appl. Catal. B: Environ*, 2017, 213, 136–146.

[43] P. She, K.L. Xu, S. Zeng, Q.R. He, H. Sun, Z.N. Liu. Investigating the size effect of Au nanospheres on the photocatalytic activity of Au-modified ZnO nanorods, *J. Colloid. Interf. Sci*, 2017, 499, 76–82.

[44] N.S. Han, D. Kim, J.W. Lee, J. Kim, H.S. Shim, Y.J. Lee, D. Lee, J.K. Song. Unexpected size effect observed in ZnO-Au composite photocatalysts, *ACS Appl. Mater. Interfaces*, 2016, 8, 1067−1072.

[45] S. Bera, J.E. Lee, S.B. Rawal, W.I. Lee. Size-dependent plasmonic effects of Au and Au@SiO_2 nanoparticles in photocatalytic CO_2 conversion reaction of Pt/TiO_2, *Appl. Catal. B: Environ*, 2016, 199, 55-63.

ACCEPTED MANUSCRIPT

Figure Captions

Fig. 1. (a) XRD patterns of $Bi_4O_5Br_2$ and Pd/$Bi_4O_5Br_2$ with different loading of Pd nanoparticles, and (b) crystal structure of $Bi_4O_5Br_2$.

Fig. 2. (a) XPS survey spectra and (b) Bi 4f, (c) O 1s, (d) Br 3d, and (e) Pd 3d XPS core-level spectra of the $Bi_4O_5Br_2$ and 1.0 wt% Pd/$Bi_4O_5Br_2$.

Fig. 3. (a) TEM and (b) HRTEM images of $Bi_4O_5Br_2$ and (c,d) TEM and (e-g) HRTEM images of 1.0 wt% Pd/$Bi_4O_5Br_2$.

Fig. 4. (a) SEM image, (b) EDS spectrum, and EDS element mapping images of O (c), Bi (d), Br (e), and Pd (f) of 1.0 wt% Pd/$Bi_4O_5Br_2$.

Fig. 5. (a) UV–Vis diffuse reflectance spectra and (b) Tauc plots of $Bi_4O_5Br_2$ and Pd/$Bi_4O_5Br_2$ composite with different amounts of Pd nanoparticles.

Fig. 6. BET specific surface area of the as-prepared $Bi_4O_5Br_2$ (a), 0.5 wt% Pd/$Bi_4O_5Br_2$ (b), 1.0 wt% Pd/$Bi_4O_5Br_2$ (c), 2.0 wt% Pd/$Bi_4O_5Br_2$ (d) and 3.0 wt% Pd/$Bi_4O_5Br_2$ (e) samples.

ACCEPTED MANUSCRIPT

Fig. 7. (a) Variation in the BPA concentration (C/C_0) versus photodegradation time and (b) ln(C_0/C) versus irradiation time of $Bi_4O_5Br_2$ and Pd/$Bi_4O_5Br_2$ composite with different amounts of Pd nanoparticles. UV–Vis spectra of BPA aqueous solution collected during the photocatalytic reactions with (c) $Bi_4O_5Br_2$ and (d) 1.0 wt% Pd/$Bi_4O_5Br_2$.

Fig. 8. Photocatalytic activities of (a) $Bi_4O_5Br_2$ and (b) 1.0 wt% Pd/$Bi_4O_5Br_2$ under monochromatic LED visible light irradiation. (c) The degradation rate and (d) pseudo-first order rate constants of $Bi_4O_5Br_2$ and 1.0 wt% Pd/$Bi_4O_5Br_2$ under monochromatic LED visible light irradiation.

Fig. 9. (a) PL spectra and (b) transient photocurrent responses (*I-t*) of $Bi_4O_5Br_2$ and 1.0 wt% Pd/$Bi_4O_5Br_2$. (c) Photodegradation efficiency of BPA in the presence of different scavengers over 1.0 wt% Pd/$Bi_4O_5Br_2$, and (d) schematic representation of the photodegradation of BPA over 1.0 wt% Pd/$Bi_4O_5Br_2$ under visible light irradiation.

ACCEPTED MANUSCRIPT

ACCEPTED MANUSCRIPT

Fig. 1

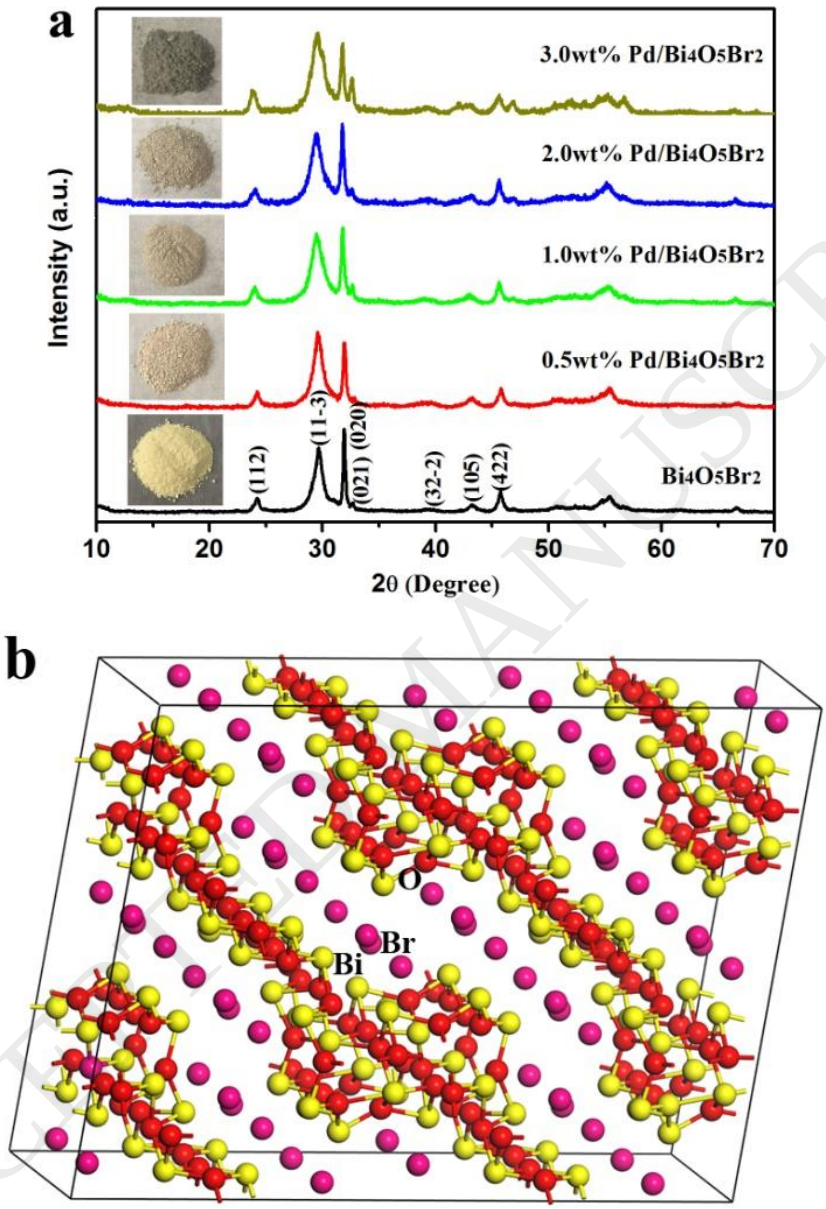

ACCEPTED MANUSCRIPT

ACCEPTED MANUSCRIPT

Fig. 2

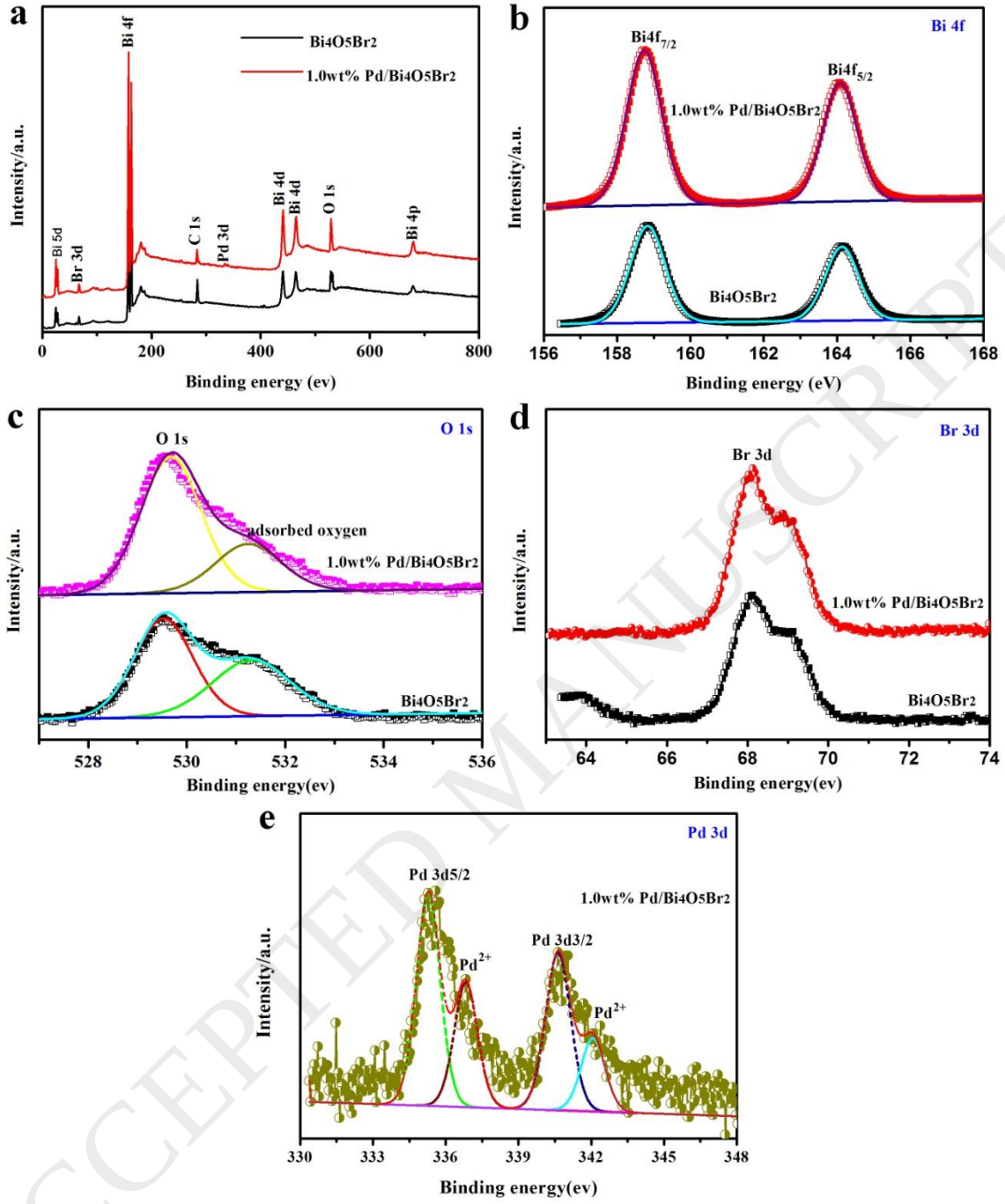

ACCEPTED MANUSCRIPT

ACCEPTED MANUSCRIPT

Fig. 3

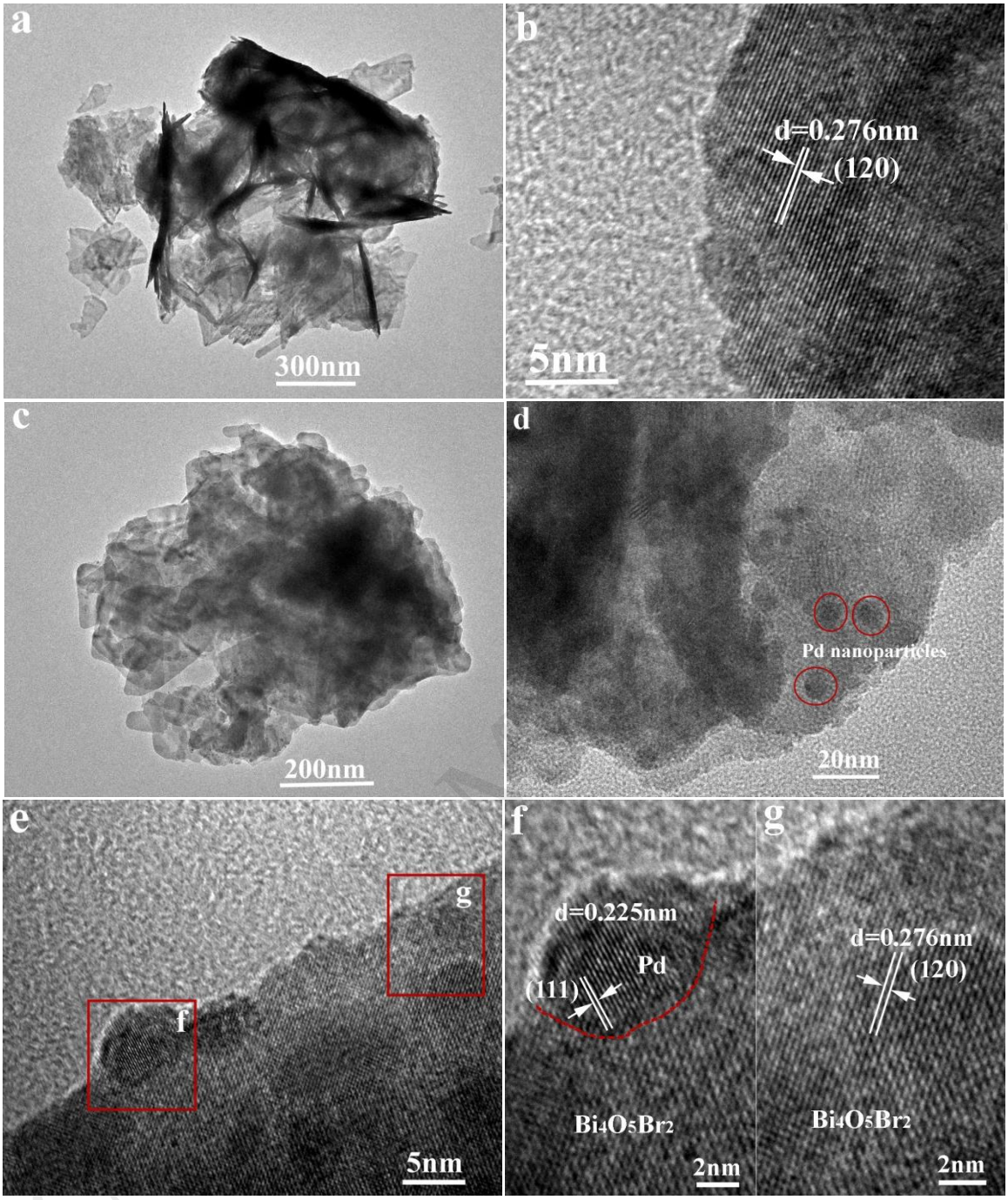

ACCEPTED MANUSCRIPT

Fig. 4

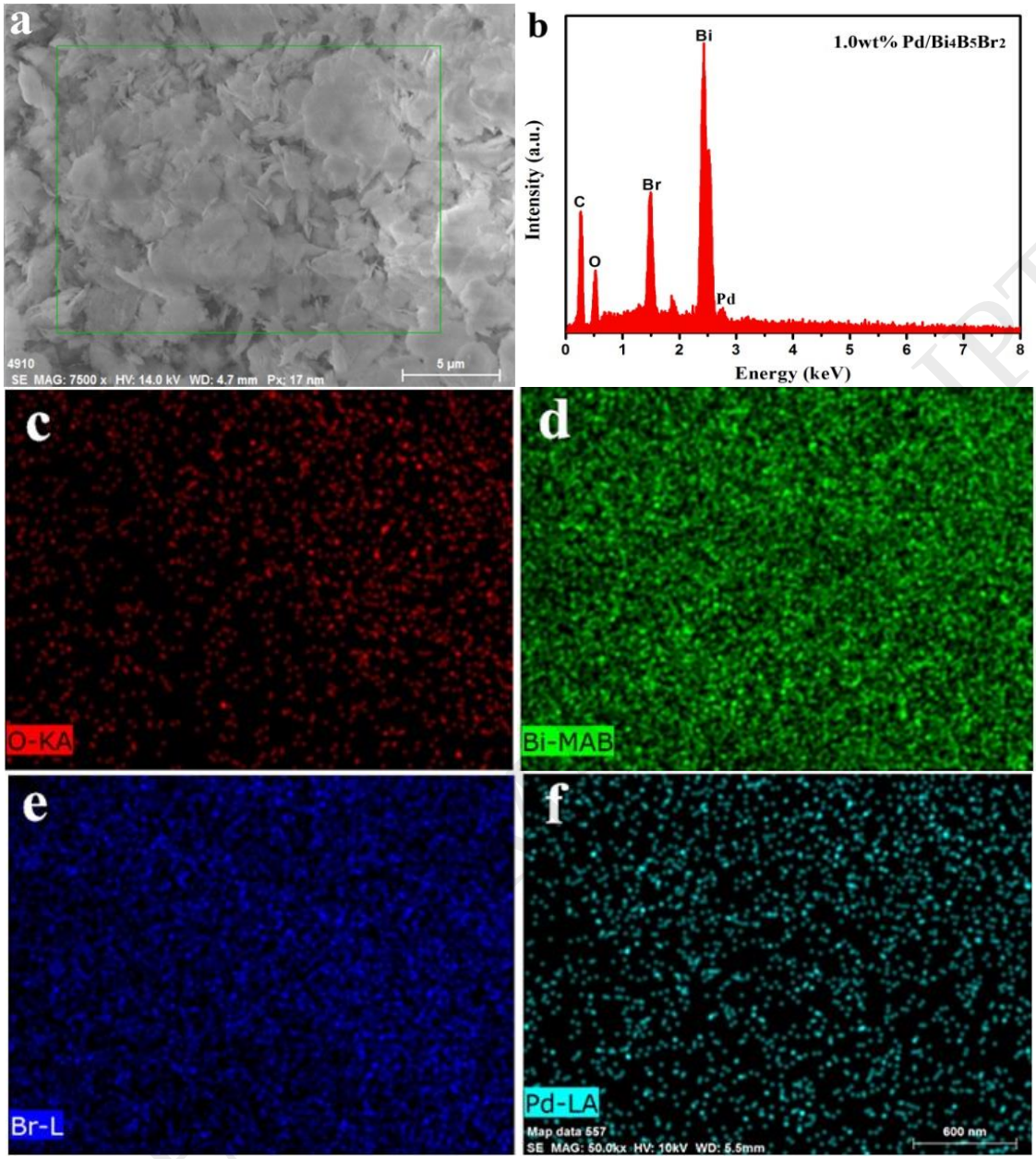

ACCEPTED MANUSCRIPT

Fig. 5

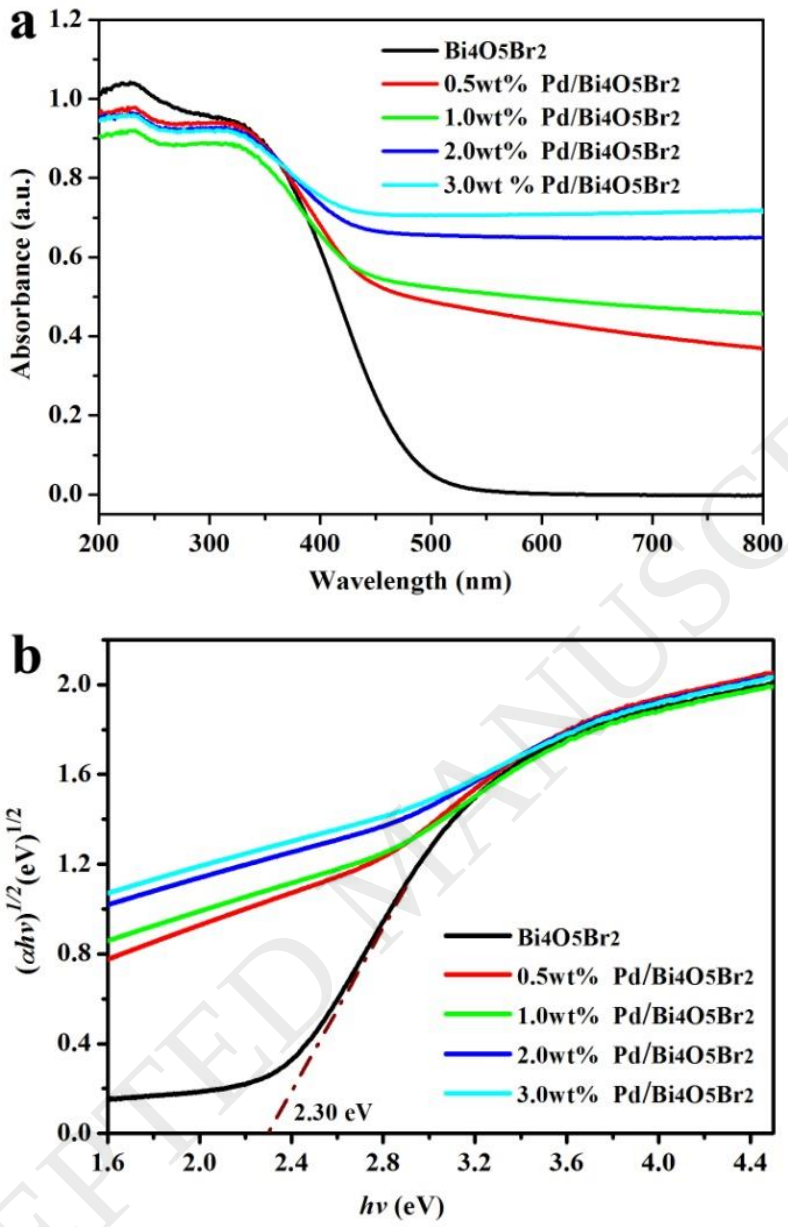

ACCEPTED MANUSCRIPT

Fig. 6

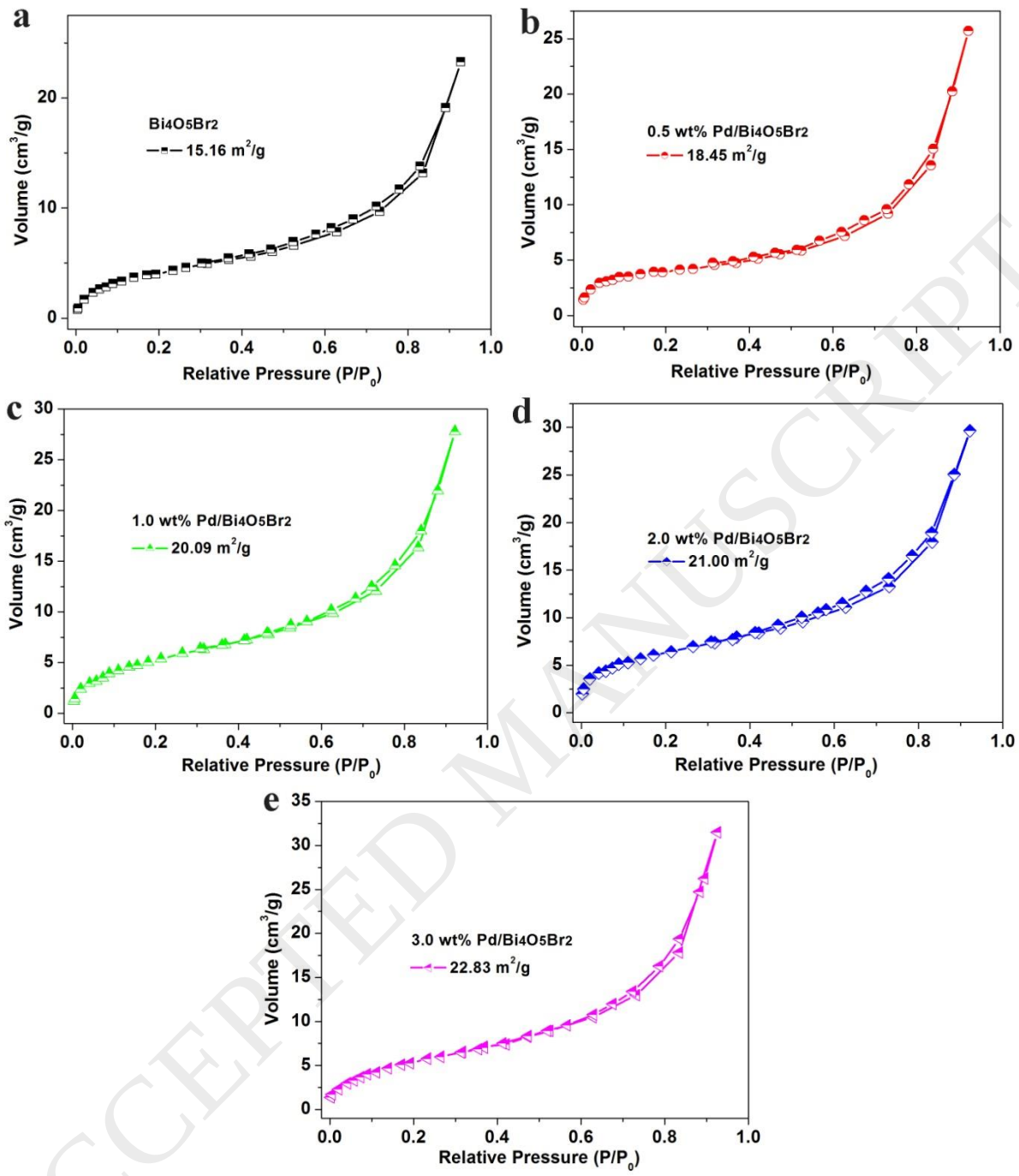

ACCEPTED MANUSCRIPT

Fig. 7

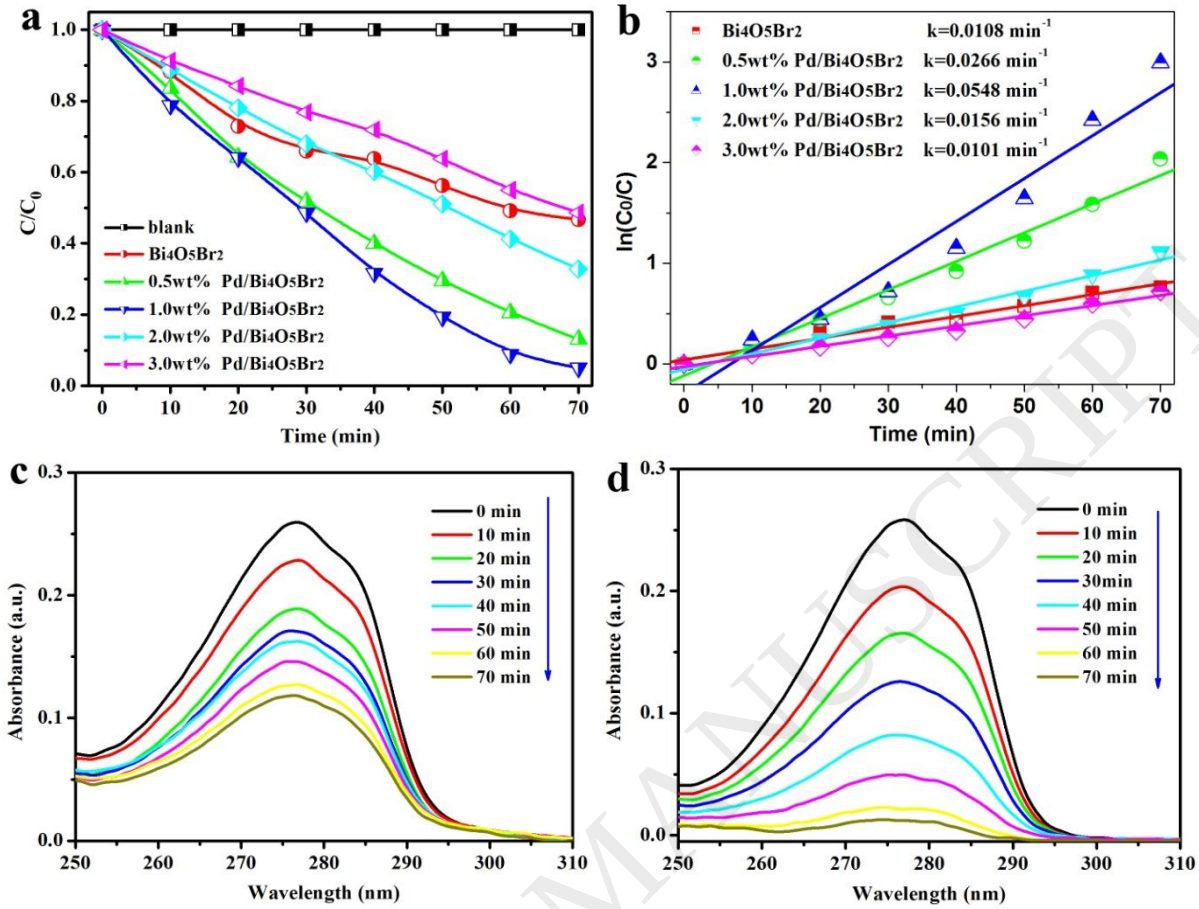

ACCEPTED MANUSCRIPT

Fig. 8

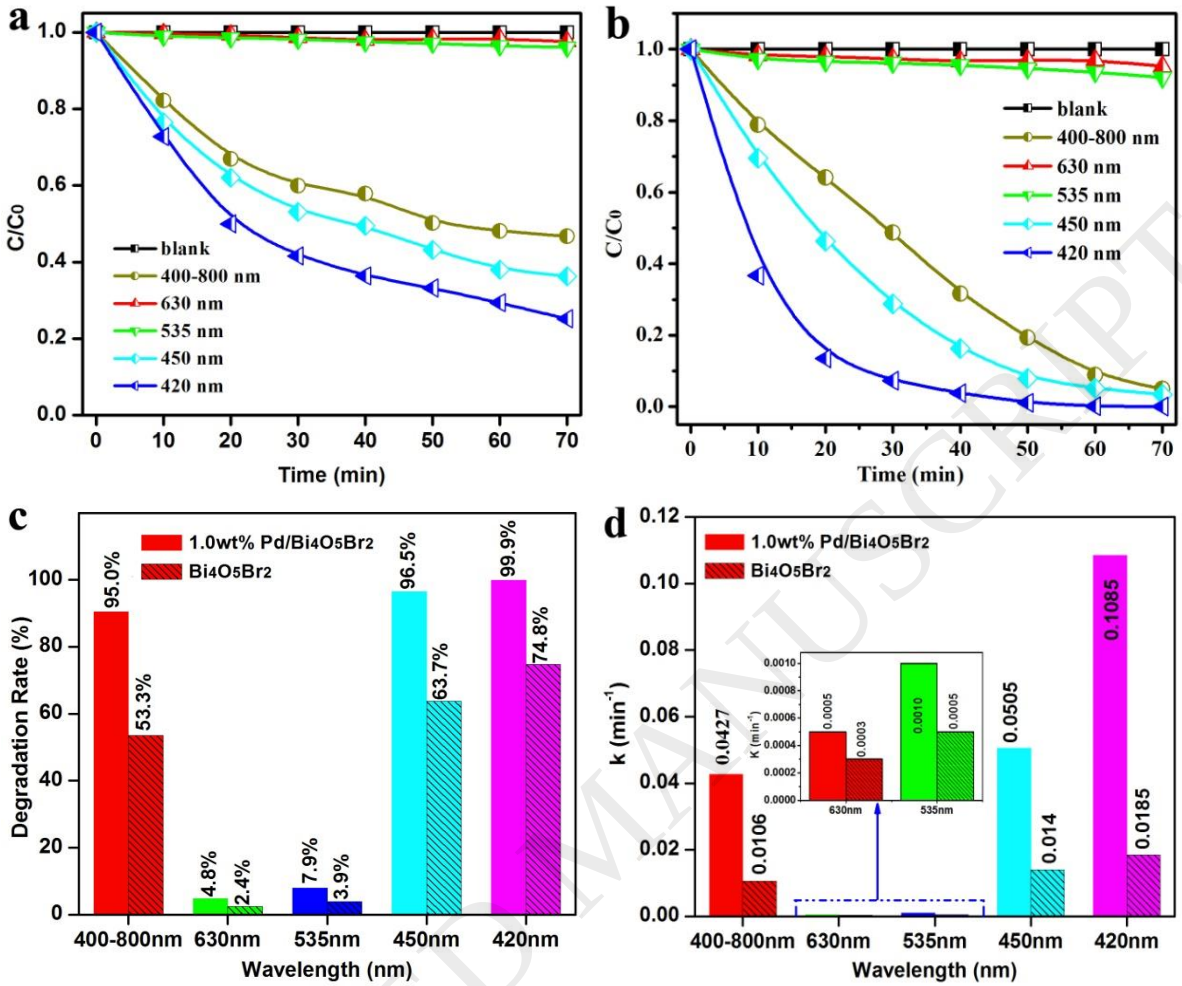

ACCEPTED MANUSCRIPT

Fig. 9